Intersecting Conical Intersection Seams: Their Location, Representation, and Effect on Local Topography

Spiridoula Matsika* and David R. Yarkony†

Department of Chemistry, Johns Hopkins University, Baltimore, Maryland 21218

Received: September 12, 2001; In Final Form: December 27, 2001

Recent work suggests that confluences, intersections between a symmetry-allowed branch and a same-symmetry branch of a seam of conical intersections are not rare occurrences. Therefore, with the goal of obtaining generalizable insights, confluences for the $1^2A' - 2^2A'$ seam of conical intersection in BH_2, and for the $1^1A - 2^1A$ seam in HNCO are examined in detail using a perturbative representation of that region. The perturbative expressions for the energy and derivative couplings in the adiabatic representation provide a means for locating confluences and evince the significant effect a confluence has on the local topography and the derivative coupling. The perturbative representation enables the derivative coupling and energy to be determined from data for either. The results obtained from the more common energy-based description are compared with those obtained from a derivative-coupling-based description.

1. Introduction

When the Hamiltonian for two conically intersecting states is extended beyond the essential linear terms to quadratic order, additional conical intersections may emerge which can lead to confluences, intersecting seams, of conical intersection. Recent work[1] suggests that confluences, intersections between a symmetry-allowed branch and a same-symmetry branch of a seam of conical intersection, rather than theoretical oddities, will have to be considered whenever a symmetry-allowed conical intersection exists. The region of the confluence requires special scrutiny because the conical topography and interstate couplings are modified in an essential manner by the confluence. Figure 1 (explained in detail below) illustrates how the topography near this point changes, depicting a point of confluence and comparing it with a standard point of conical intersection. These changes can have important consequences in the dynamics along that surface. Motivated by the potential impact of these confluences, here we consider their location, topography, and analytic representation.

Confluences are a subspace of a symmetry-allowed seam with dimension one less than the dimension of this seam. In a triatomic molecule, the confluence is a point. This point can be located by using a previously introduced method, which searches along the symmetry-allowed seam which is a line. In larger molecules, the confluence is a multidimensional subspace and such a search becomes cumbersome. An iterative method discussed here is based on analytic representations of the potential energy surfaces and derivative couplings, and can locate multidimensional subspaces of confluences systematically, unlike the previously noted approach which locates points of confluence one at a time. The analytic representations are derived using a previously introduced approach based on second-order degenerate perturbation theory.

Conical intersections are often thought of as difficult to describe in the adiabatic representation because the derivative couplings become singular. An advantage of the present representation is that the singularities in the adiabatic basis appear in the first order perturbative terms and can be subtracted out leaving the well-behaved, second and higher order, terms

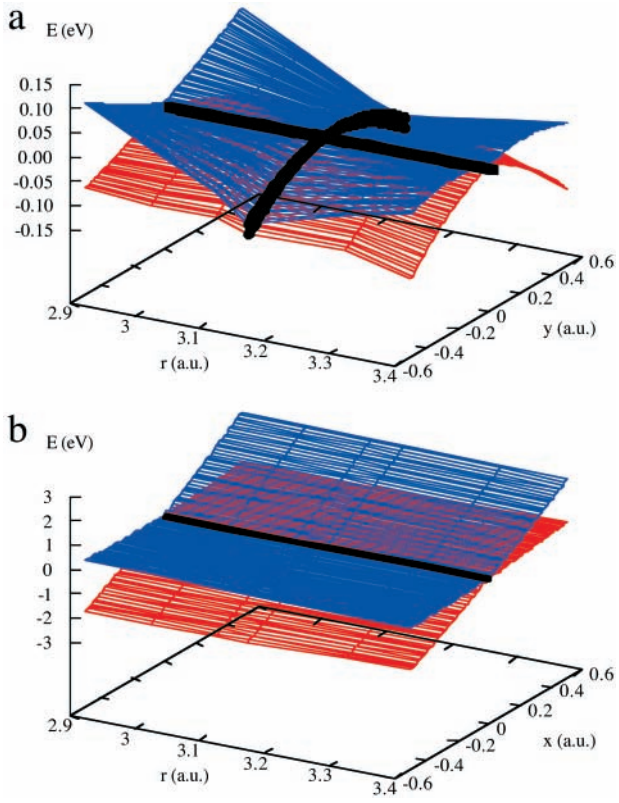

Figure 1. (a) Energies $E_{1^2A'}$, $E_{2^2A'}$ of the two intersecting states in BH_2 along r (approximately the seam coordinate in the C_{2v} seam) and intersection adapted coordinate y close to the confluence. For points of conical intersection along the seam the first and second-order parameters were used to calculate the energies on the g−h plane. The two black lines correspond to the degenerate energies along the C_{2v} seam and the degenerate energies along the C_s seam. The confluence is where the two lines cross. (b) The energies $E_{1^2A'}$, $E_{2^2A'}$ vs (r,x). The zero of the energy is along the seam at $x = 0$ or $y = 0$.

* To whom correspondence should be addressed. E-mail address: smatsika@jhunix.hcf.jhu.edu.

† E-mail address: yarkony@jhuvms.hcf.jhu.edu.

10.1021/jp0134897 CCC: $22.00
Published on Web 02/16/2002

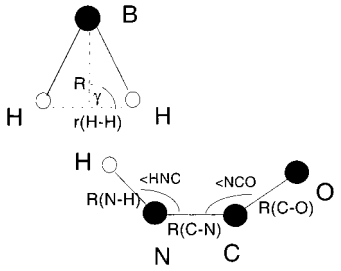

Figure 2. Jacobi and internal coordinates for the systems BH_2 and cis HNCO, respectively.

to be described. Although first order terms are generally predominant near a conical intersection, second order terms may significantly modify the topography as the distance from the conical intersection increases. However, near a confluence the first-order terms become small so the second-order terms may be preeminent. The perturbative representation is related to a common method for describing interacting potential energy surfaces and derivative couplings, the Double Many Body Expansion (DMBE).[2−6] In this approach, the ab initio energy data are used to determine the DMBE parameters which in turn are used to calculate derivative couplings. There is little information on the reliability of the derivative couplings obtained in this way. Some comparisons have been made for H_3.[6] In the present representation, we can both determine, and assess the reliability of, the representation.

This work will be used to consider the $1^2A'$, $2^2A'$ states in BH_2[7] and 1^1A, 2^1A states in cis HNCO[8] for which confluences are known. These systems are shown in Figure 2. For BH_2 continuous parametrizations of the potential energy, and the interstate coupling, surfaces in both the adiabatic and diabatic representations will be determined and the topography of the intersecting seams will be carefully analyzed. This analysis forms part of an ongoing project to provide potential energy, and derivative coupling, surfaces of the 1, $2^2A'$ and $1^2A''$ states.[9] It will be shown that both first and second order parameters can be chosen continuous along the branches of the seam and join smoothly at the confluence. Continuity is an important issue. Non-continuous parameters would only give analytic representations at discrete points of the surface with no way of interpolating between them. Two methods of obtaining the parameters, the energy-based (e-method) and the derivative-coupling-based (f-method), will be compared. In the e-method (f-method) energy data (derivative coupling data) is used to determine the parameters.

For BH_2 (cis-HNCO) the confluence (points on the subspace of the confluence) will be located using an iterative approach based on the derivative coupling-based parametrization. The potential power in this method is evinced in the treatment of HNCO where the high dimensionality makes the location of confluences impossible using the pointwise algorithm.

In addition to being valuable tools in the study of intersecting seams, the above molecules are of practical importance. The $1,2^2A'$ and $1^2A''$ potential energy surfaces of BH_2 are relevant to the stability of the van der Waals complex $B-H_2$ formed when B is used as a dopant in a cryogenic H_2 and the ultimate fate of the H_2 upon combustion.[7,10−14] The portion of the 1^1A-2^1A seam of HNCO in a cis configuration is relevant to the vibronic stability of cis HNCO on S_1 which has yet to be observed.

Section 2 reviews the theoretical approach, whereas section 3 presents the results of the numerical study. Section 4 concludes and discusses directions for future research.

2. Theory

Conical intersections do not exist as isolated points but as continuous seams of dimension $N^{\text{int}} - 2$ for the nonrelativistic Coulomb Hamiltonian, where N^{int} is the number of internal coordinates. Degenerate perturbation theory, originally developed by Mead to describe X_3 systems,[15,16] can be used for the analysis of the vicinity of conical intersections where symmetry plays no role. Details of this approach have been reported previously.[15,17] Here, it is reviewed and extended.

2.1 g−h Plane and Intersection Adapted Coordinates. The degeneracy of a conical intersection of states I, J, at $\mathbf{R}^x$ is lifted in a linear manner in the g−h or branching plane,[18,19] a plane perpendicular to the seam defined by the axes $\mathbf{x} = \mathbf{g}^{IJ}/g$ (tuning mode) and $\mathbf{y} = \mathbf{h}^{IJ}/h$ (coupling mode)[20] where $g = ||\mathbf{g}^{IJ}||$, $h = ||\mathbf{h}^{IJ}||$

$$\mathbf{2g}^{IJ}(\mathbf{R}) = \mathbf{c}^I(\mathbf{R}^x)[\nabla\mathbf{H}(\mathbf{R})]\mathbf{c}^I(\mathbf{R}^x) - \mathbf{c}^J(\mathbf{R}^x)[\nabla\mathbf{H}(\mathbf{R})]\mathbf{c}^J(\mathbf{R}^x) \quad (1)$$

$$\mathbf{h}^{IJ}(\mathbf{R}) = \mathbf{c}^I(\mathbf{R}^x)[\nabla\mathbf{H}(\boldsymbol{R})]\mathbf{c}^J(\mathbf{R}^x) \quad (2)$$

Here, $\mathbf{c}^I$ are the expansion coefficients of the adiabatic wave functions $\Psi_I = \sum_{a=1}^{CSF} c_a^I\, \psi_a$ in the configuration state function (CSF) basis[21] and satisfy the equation $[\mathbf{H}(\mathbf{R}) - E_I(\mathbf{R})]\mathbf{c}^I(\mathbf{R}) = 0$, where $\mathbf{H}(\mathbf{R})$ is the electronic Hamiltonian in the CSF basis. The degenerate electronic wave functions have been chosen such that $\mathbf{x} \cdot \mathbf{y} = 0$. It is particularly convenient to describe the vicinity of a conical intersection in terms of the orthogonal intersection adapted coordinates[22] defined as the cylindrical polar coordinates ρ, θ, z_i where $x = \rho\cos\theta$, $y = \rho\sin\theta$, and z_i are displacements in the directions $\mathbf{x}$, $\mathbf{y}$, and $\mathbf{z}^{\mathbf{i}}$, respectively. The $N^{\text{int}} - 2$ mutually orthogonal internal coordinates $\mathbf{z}^{\mathbf{i}}$ describe the seam, the orthogonal complement of the g−h plane. In the following discussion, a point given either in (x, y, $\mathbf{z}^{\mathbf{i}}$) or (ρ, θ, $\mathbf{z}^{\mathbf{i}}$) coordinates will be denoted as $\boldsymbol{\tau}$.

2.2 Adiabatic Energies. The diagonal adiabatic Hamiltonian is given through second order in perturbation theory by[22]

$$\mathbf{H}^{ad,(2)}(\mathbf{R}) = (E_I(\mathbf{R}^x) + s^{IJ}(\mathbf{R})\cdot\delta\mathbf{R} + N(\mathbf{R}))\mathbf{I} + [-\rho q(\theta) + A(\mathbf{R})\cos\lambda - B(\mathbf{R})\sin\lambda]\boldsymbol{\sigma}_z \quad (3)$$

where $\mathbf{I}$ is the 2×2 unit matrix, $\boldsymbol{\sigma}_z$ a Pauli matrix and

$$q(\theta)^2 = g^2\cos^2\theta + h^2\sin^2\theta \quad (4)$$

$$2\mathbf{s}^{IJ}(\mathbf{R}) = \mathbf{c}^I(\mathbf{R}^x)[\nabla\mathbf{H}(\mathbf{R})]\mathbf{c}^I(\mathbf{R}^x) + \mathbf{c}^J(\mathbf{R}^x)[\nabla\mathbf{H}(\boldsymbol{R})]\mathbf{c}^J(\mathbf{R}^x) \quad (5)$$

$\lambda(\theta)$ is given by

$$g\cos\theta = q(\theta)\cos\lambda\,(\theta)$$

$$h\sin\theta = q(\theta)\sin\lambda\,(\theta) \quad (6)$$

and $s_w = \mathbf{s}^{IJ}\cdot\mathbf{w}$, $w = x, y, z_i$. N, A, B, which define the second-order energy, are given by

$$N(\mathbf{R}) = \eta(\rho, \theta, \mathbf{z}; \mathbf{n}) + \sum_{i,j} n_3^{(z_iz_j)} z_i z_j \quad (7)$$

where

$$\eta(\rho, \theta, \mathbf{z}; \mathbf{n}) = \rho^2 N^{(\rho)}(\theta) + \rho\sum_i z_i N^{(z_i)}(\theta)$$

$$N^{(\rho)}(\theta) = n_1^{(\rho)}\cos^2\theta + n_2^{(\rho)}\sin^2\theta + n_3^{(\rho)}\cos\theta\sin\theta$$

$$N^{(z_i)}(\theta) = n_1^{(z_i)}\cos\theta + n_2^{(z_i)}\sin\theta$$

$A(\mathbf{R}) = \eta(\rho, \theta, \mathbf{z}; \mathbf{a})$, $B(\mathbf{R}) = \eta(\rho, \theta, \mathbf{z}; \mathbf{b})$ and

$$\mathbf{n} = (n_1^{(\rho)}, ..., n_2^{(z_i)})$$

Using the above Hamiltonian the energy difference $\Delta E_{JI} \equiv E_J - E_I$ at a point x, y, $\mathbf{z}$ away from $\mathbf{R}^x$, the point of conical intersection of states I and J, is given in first and second order respectively by

$$\Delta E_{JI}^{(1)} = E_J^{(1)} - E_I^{(1)} = 2\rho q(\theta) \tag{8}$$

$$\Delta E_{JI}^{(2)} = E_J^{(2)} - E_I^{(2)} = -2(A\cos\lambda - B\sin\lambda) \tag{9}$$

In the following discussion, the subscripts JI in ΔE_{JI} will be omitted. Note that $\Delta E = 0$ for all $\boldsymbol{\tau}$ with $x = y = 0$. This is referred to as the linear seam approximation and leads to a piecewise linear approximation to the seam.

2.3 Derivative Couplings. The derivative couplings are defined as

$$f_R^{IJ}(\mathbf{R}) = \left\langle \Psi^I(\mathbf{r}; \mathbf{R}) \middle| \frac{\partial \Psi^J(\mathbf{r}; \mathbf{R})}{\partial R} \right\rangle_{\mathbf{r}} \tag{10}$$

They consist of two parts, the configuration interaction (CI) contribution (${}^{CI}f_R^{IJ}$) and the much smaller CSF contribution (${}^{CSF}f_R^{IJ}$).[23] A and B, which are related to $\Delta E^{(2)}$ by eq 9 are also related to ${}^{CI}f_R^{IJ}(\mathbf{R})$ as follows

$${}^{CI}f_\rho(\theta) \approx f_\rho^{(2)}(\theta) = -\frac{M^{(\rho)}(\theta)}{2q(\theta)}, \quad f_{z_i}^{(2)}(\theta) = -\frac{M^{(z_i)}(\theta)}{2q(\theta)} \tag{11}$$

$${}^{CI}f_\theta(\rho, \theta, \mathbf{z}) \approx f_\theta^{(2')}(\rho, \theta, \mathbf{z}) = f_\theta^{(1)}(\theta) - f_\theta^{(2)}(\rho, \theta, \mathbf{z}) \tag{12}$$

where

$$f_\theta^{(1)}(\theta) = (\partial/\partial\theta)\lambda(\theta)/2,$$
$$f_\theta^{(2)}(\rho, \theta, \mathbf{z}) = (\partial/\partial\theta)(\rho f_\rho^{(2)}(\theta) + \sum_i z_i f_{zi}^{(2)}(\theta)) \tag{13}$$

and

$$M^{(t)}(\theta) = A^{(t)}(\theta)\sin\lambda(\theta) + B^{(t)}\cos\lambda(\theta),\ t = \rho, z_i \tag{14}$$

Below the superscripts IJ and CI will be omitted when no confusion will arise. The advantage of using the orthogonal intersection adapted coordinates is that the only singular part of the derivative coupling is $(1/\rho)f_\theta^{(1)}$.

The first order energy difference and derivative coupling can be obtained from information only at $\mathbf{R}^x$, using eqs 1, 2, 3. Perturbation theory provides explicit expressions for the computation of $A(\mathbf{R})$, $B(\mathbf{R})$, and $N(\mathbf{R})$.[22] However, these expressions are very costly computationally and simpler, less costly, methods are desirable. N can be determined only from the energy. On the other hand, A and B determine, and hence can be determined, from the energies and derivative couplings. However, identical results are not expected because (i) ${}^{CSF}f_R^{IJ}$ is not included in the A and B, (ii) the second order energy is only known approximately, and (iii) seam curvature is only included in a piecewise linear manner. The final effect is specific to the present perturbative analysis but the first two effects are present in most common energy based approaches for describing potential energy surfaces. Thus, their study is of general interest. To address these issues, here we consider the A and B determined from both energies and derivative couplings. $a_i^{(\rho)}$, $b_i^{(\rho)}$ can be determined from the energy data whereas all $\mathbf{a}$, $\mathbf{b}$ can be determined from the derivative coupling data.

2.4 Diabatic Representation. From eqs 11 and 13 and the commutation of the partial derivative operators we have $(\partial/\partial\rho)f_\theta^{(2)}(\rho, \theta, \mathbf{z}) = (\partial/\partial\theta)(f_\rho^{(2)}(\theta))$ and $(\partial/\partial z_i)f_\theta^{(2)}(\rho, \theta, \mathbf{z}) = (\partial/\partial\theta)(f_{zi}^{(2)}(\theta))$ so that the derivative coupling in eqs 11, 12, 13 is removable by a rotation by the angle

$$\Theta(\rho, \theta, \mathbf{z}) = \lambda(\theta)/2 + \sum_i \frac{z_i M^{(z_i)}(\theta)}{2q(\theta)} + \frac{\rho M^{(\rho)}(\theta)}{2q(\theta)} \tag{15}$$

Rotating the adiabatic Hamiltonian $\mathbf{H}^{ad,(2)}$ in eq 3 gives to second order[22]

$$\mathbf{H}^{d,(2)}(\mathbf{R}) = (E(\mathbf{R}^x) + \mathbf{s}(\mathbf{R})\cdot\delta\mathbf{R} + N(\mathbf{R}))\mathbf{I} + G(x, y, \mathbf{z})\boldsymbol{\sigma}_z + V(x, y, \mathbf{z})\boldsymbol{\sigma}_x \tag{16}$$

where

$$G(x, y, \mathbf{z}) = -g\rho\cos\theta + \eta(\rho, \theta, \mathbf{z}; \mathbf{a}) \tag{17}$$

$$V(x, y, \mathbf{z}) = h\rho\sin\theta + \eta(\rho,\theta, \mathbf{z}; \mathbf{b}) \tag{18}$$

$\mathbf{H}^{d,(2)}$ is in turn diagonalized by a rotation by the Θ' which satisfies

$$\tan 2\Theta' = \frac{V(x, y, \mathbf{z})}{G(x, y, \mathbf{z})} \tag{19}$$

Expanding eq 19 to second order in ρ and z_i

$$\tan 2\Theta' \approx -\tan\lambda - \left(\frac{\eta(\rho, \theta, \mathbf{z}; \mathbf{a})}{q(\theta)}\sin\lambda + \frac{\eta(\rho, \theta, \mathbf{z}; \mathbf{b})}{q(\theta)}\cos\lambda\right)\frac{1}{\cos^2\lambda} \tag{20}$$

Using the approximation for small ϵ, $\tan(\lambda + \epsilon) \approx \tan\lambda + (\epsilon/\cos^2\lambda)$, one gets $\Theta = -\Theta'$, to first order in ρ and z_i as expected, since, as discussed elsewhere, the basis for $\mathbf{H}^d$ is quasidiabatic.[24]

From eq 16 the energy difference is given by

$$\Delta E = 2[\rho^2 q^2 + A^2 + B^2 - 2\rho q(A\cos\lambda - B\sin\lambda)]^{1/2} \tag{21}$$

which becomes to second order

$$\Delta E \approx 2(\rho q - A\cos\lambda + B\sin\lambda) \tag{22}$$

identical to the adiabatic expression (eqs 8, 9).

2.5 Determining A and B. As noted above $A(\rho, \theta, \mathbf{z})$ and $B(\rho, \theta, \mathbf{z})$ can be determined from either the second-order energy difference or the derivative coupling. For $\mathbf{R}$ in the g−h plane

$$\frac{q(\theta)}{(-2\rho^2)}(\Delta E/q(\theta) - 2\rho) \approx (A^{(\rho)}\cos\lambda(\theta) - B^{(\rho)}\sin\lambda(\theta)) \tag{23}$$

$$-2f_w q(\theta) \approx (A^{(w)}(\theta)\sin\lambda(\theta) + B^{(w)}\cos\lambda(\theta)),\ w = \rho, z_i \tag{24}$$

The results of the previous section show that eqs 23 and 24 for $w = \rho$ are equivalent through terms of order ρ^2 in the perturbation expansion. However, $1/q(\theta)$ and f_ρ can be sharply peaked and eqs 23 and 24 need not give equivalent results in

practical situations. In this work, the second-order coefficients are obtained from the solution of the linear least squares problem

$$\frac{\partial}{\partial\alpha}\sum_n [-2f_w(\mathbf{R}_n)q(\theta_n) - (A^{(w)}(\theta_n)\sin\lambda(\theta_n) + B^{(w)}(\theta_n)\cos\lambda(\theta_n))]^2 = 0,\ \alpha = a_j^{(w)}, b_j^{(w)},\ w = \rho, z_i \quad (25)$$

or the equivalent expression arising from eq 23, along loops in the g−h plane. n is the number of points collected along the loop, defined by $\rho = \rho^0$, $\theta = \theta_1, \theta_2, \ldots\theta_n$. In order for perturbation theory to be valid ρ^0 should be small; if it is too small, however, numerical problems may result. Because $1/\rho f_\theta$ is singular, whereas f_ρ is not, the ρ direction must be known with sufficient precision so that contamination of f_ρ by $1/\rho f_\theta$ is negligible. Thus a balanced value is desired. Here, $\rho^0 = 0.05$ a_0 was used. The parameters depend also on n. Using $n = 17$, at equal intervals for θ of 22.5°, provides results that are converged with respect to n.

2.6 Confluences. *2.6.1 Defining Equations*. Using the Hamiltonian in eq 16 the seam of conical intersections satisfies $G(x, y, \mathbf{z}) = V(x, y, \mathbf{z}) = 0$. However, if V is factorable, $V = V^{(1)}V^{(2)}$, then the seam conditions yield two pairs of equations, $G = V^{(1)} = 0$ and $G = V^{(2)} = 0$, defining two branches of the seam. A confluence occurs when

$$G = V^{(1)} = V^{(2)} = 0 \quad (26)$$

We consider the case described in the Introduction in which there is a different symmetry branch and consider the least restrictive case, which is the spatial point group C_s with electronic states carrying irreducible representations A' and A''. Then on the different symmetry seam we can require, without loss of generality, $\mathbf{x} \sim A'$ and $\mathbf{y} \sim A''$, where $\sim$ denotes "transforms as". Similarly, the internal coordinates can be partitioned into N^s A' or symmetry preserving modes and $N^a = N^{int} - N^s$ A'' or symmetry breaking modes. It then follows that $a_3^{(\rho)} = b_1^{(\rho)} = b_2^{(\rho)} = 0$ and all $a_2^{(z_i)}$, $b_1^{(z_i)}$ for which $z_i \sim A'$ must vanish, so that V becomes

$$V(x, y, \mathbf{z}) = hy + b_3^{(\rho)}xy + \sum_{i=1}^{N^a-1} b_1^{(z_i)}xz_i + \sum_{j=N^a+1}^{N^{int}} b_2^{(z_j)}yz_j \quad (27)$$

This is clearly not factorable unless the $b_1^{(z_i)}$ vanish. In a N atom molecule constrained to planarity $N^s = 2N - 3$. Thus, for a tetra atomic $N^a = 1$, there are no $b_1^{(z_i)}$ terms, and V is factorable. A similar situation occurs in a tri atomic molecule for C_{2v} symmetry where $N^a = 1$ and $N^s = 2$. For a penta atomic molecule however there is one $b_1^{(z_i)}$, so that V is only factorable in the subspace where $z_i = 0$.

When V is factorable the solution to eq 26 using eq 27 is

$$\bar{\mathbf{z}} = (d_{N^a+1}\zeta_{N^a+1}, \ldots, d_{N^{int}}\zeta_{N^{int}}) \text{ with } \sum_{i=N^a+1}^{N^{int}} d_i = 1 \quad (28)$$

where

$$\zeta_i = -h/b_2^{(z_i)} \quad (29)$$

Because $\bar{\mathbf{z}}$ is an $N^s - 1$-dimensional vector subject to one constraint the maximum dimension of the confluence is $N^s - 2$. It can be shown that $\mathbf{h}^{IJ}(\boldsymbol{\tau}^{dx} \rightarrow \boldsymbol{\tau}^c) \cdot \mathbf{h}^{IJ}(\boldsymbol{\tau}^{sx} \rightarrow \boldsymbol{\tau}^c) = 0$ where $\boldsymbol{\tau}^{dx}$ is a point of conical intersection on the different symmetry seam, $\boldsymbol{\tau}^{sx}$ is a point of conical intersection on the same symmetry seam and $\boldsymbol{\tau}^c$ is a point of confluence. Further, because $G = 0$ on both branches of the seam and $\nabla G = \mathbf{g}^{IJ}$, at the confluence $\mathbf{g}^{IJ}(\boldsymbol{\tau}^{dx} \rightarrow \boldsymbol{\tau}^c) \cdot \mathbf{g}^{IJ}(\boldsymbol{\tau}^{sx} \rightarrow \boldsymbol{\tau}^c) \rightarrow g^2(\boldsymbol{\tau}^c)$. Thus, the limiting direction of $\mathbf{g}^{IJ}$ at $\mathbf{R}^c$ is the same in the two branches. However, the limiting directions $\mathbf{h}^{IJ}(\boldsymbol{\tau}^{sx})$ and $\mathbf{h}^{IJ}(\boldsymbol{\tau}^{dx})$ are orthogonal. Because all directions orthogonal to $\mathbf{h}^{IJ}$, apart from $\mathbf{g}^{IJ}$, are $\mathbf{z}^i$ directions it follows that $\mathbf{h}^{IJ}(\boldsymbol{\tau}^{sx})$ approaches a $\mathbf{z}^i$ direction in the different-symmetry branch and $\mathbf{h}^{IJ}(\boldsymbol{\tau}^{dx})$ approaches a $\mathbf{z}^i$ direction in the same-symmetry branch. Because the maximum dimension of the branching space is two, $|\mathbf{h}^{IJ}(\boldsymbol{\tau}^{dx} \rightarrow \boldsymbol{\tau}^c)| = |\mathbf{h}^{IJ}(\boldsymbol{\tau}^{sx} \rightarrow \boldsymbol{\tau}^c)| = 0$. Equivalently, $\mathbf{h}^{IJ} = V^{(1)}\nabla V^{(2)} + V^{(2)}\nabla V^{(1)} = 0$ when $V = V^{(1)}V^{(2)}$ and $V^{(1)} = V^{(2)} = 0$. $\nabla V^{(1)}$ and $\nabla V^{(2)}$ here are $\mathbf{h}^{IJ}$ for the two different branches of the seam. For a triatomic molecule, as BH_2, there is only one $\mathbf{z}$ direction so $\mathbf{h}^{IJ}$ and $\mathbf{z}$ are interchanged in the two branches.

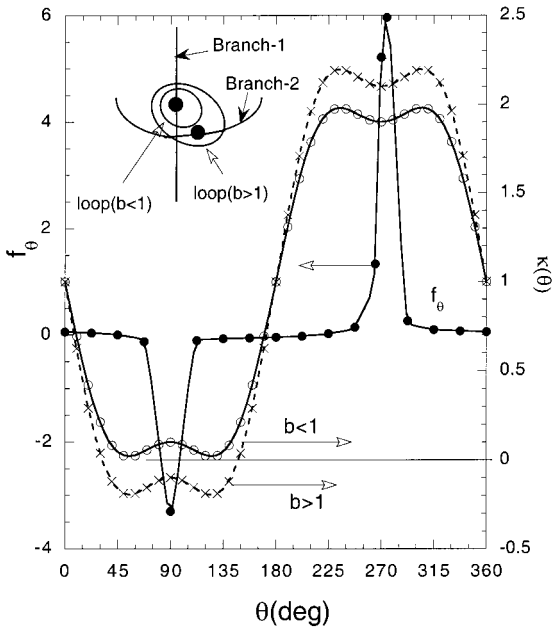

Figure 3. Function from eq 33 $\kappa(\theta) = (1 - b\sin\theta(a + \cos^2\theta))$ for $b = 1.1$ (crosses) and 0.9 (circles). Also for HNCO, f_θ along a circle of radius 0.05 a_0 centered at $\mathbf{R}^x$ = (R(H−N), 2.67, 2.271, 107, 106, 0.015) is shown, in a plane tilted with respect to the g−h($\mathbf{R}^x$).

It is the vanishing of h that leads to the unique topography observed in Figure 1 and discussed further below. Note too that in the $\mathbf{h}^{IJ}$ direction the linear contributions are necessarily subordinate to the quadratic terms. The implications of this are discussed in Section 3.

2.6.2 Geometric Phase Effect. An important aspect of a confluence is its suppression of the geometric phase effect. Consider a point of conical intersection on the symmetry-allowed seam, $\boldsymbol{\tau}^{sx}$. In general, the circulation of the derivative coupling along an infinitesimal loop containing that point is equal to π. However, when $\boldsymbol{\tau}^{sx}$ is near a confluence this need not be the case. A loop in a plane tilted with respect to the g−h plane, centered at $\boldsymbol{\tau}^{sx}$, can, even for small loops, contain two points of conical intersection, one on the same symmetry branch and one on the different symmetry branch (See Figure 3). For such a loop there is no net geometric phase effect. This can be understood using the simplified $\mathbf{H}^d$, with $\mathbf{a}^{(\rho)} = \mathbf{b}^{(\rho)} = \mathbf{a}^{(z_i)} = \mathbf{b}^{(z_j)} = 0$ for all $\mathbf{a}^{(z_i)}$ and for all but one $\mathbf{b}^{(z_j)}$, so that

$$G = gx \text{ and } V = hy + b^{(z)}yz \quad (30)$$

Consider a loop in the (x, y') plane, a plane rotated about the x-axis of the g−h plane by an angle α, that is

$$\begin{pmatrix} y' \\ z' \end{pmatrix} = \begin{pmatrix} \cos\alpha & -\sin\alpha \\ \sin\alpha & \cos\alpha \end{pmatrix} \begin{pmatrix} y \\ z \end{pmatrix} \tag{31}$$

Then, in terms of (ρ, θ), where $x = \rho\cos\theta$, $y' = \rho\sin\theta$ eq 30 becomes

$G = (g\rho)\cos\theta$ and

$$V = (h\cos\alpha)\,\rho\sin\theta(1 - (b^{(z)}/h)\sin\alpha\,\rho\sin\theta) \tag{32}$$

From eq 19 Θ satisfies

$$2\frac{\partial}{\partial\theta}\Theta \equiv 2f_\theta^{(p)} = \frac{\kappa(\theta)}{\dfrac{g\cos^2\theta}{h\cos\alpha} + \dfrac{h\cos\alpha\sin^2\theta}{g}\left(1 - \rho\dfrac{b^{(z)}}{h}\sin\alpha\sin\theta\right)^2} \tag{33}$$

where

$$\kappa(\theta) = \left(1 - \frac{b^{(z)}}{h}\sin\alpha\,\rho\sin\theta(1 + \cos^2\theta)\right) \tag{34}$$

As noted previously $f_\theta^{(p)} \approx f_\theta \equiv \langle\Psi_J^a|(\partial/\partial\theta)|\Psi_I^a\rangle_r$. For $\rho \rightarrow 0$ (see loop 1 in Figure 3), $\kappa(\theta) \rightarrow 1$, $f_\theta^{(p)}$ is strictly positive, its circulation[17,25] $\chi(f_\theta^{(p)}) = \int_0^{2\pi} f_\theta^{(p)} d\theta = \Theta(2\pi) - \Theta(0) = \pi$. This infinitesimal circle encloses exactly one point of conical intersection at the origin, $(\rho, \theta) = (0, \theta)$. However, for $\rho b^{(z)}\sin\alpha/h > 1$ the circle encloses two conical intersections (see loop 2 in Figure 3), at $(0, \theta)$ and $(h/(b^{(z)}\sin\alpha), \pi/2)$; $\kappa(\theta)$ has two zeros (see Figure 3) so that $f_\theta^{(p)}$ changes sign twice. As a consequence, $\Theta(2\pi) = \Theta(0)$, and there is no net geometric phase effect. This point will be illustrated with ab initio calculations below.

2.7 Locating Confluences. There are two ways the perturbation theory expressions above can be used to locate confluences. The first approach uses the fact that the coupling matrix element h becomes zero when the two different branches intersect. For a tri atomic molecule by plotting h along the symmetry-allowed seam one can determine whether a confluence exists. The principal limitation to this approach is that it becomes cumbersome to use when $N^{\text{int}} > 3$ owing to the increased dimension of the symmetry-allowed seam.

An alternative, potentially more powerful, approach for determining the locus of confluences is based on eqs 28,29. Although this approach, unlike that based on h, requires knowledge of the second-order parameters, it can determine the locus of confluences in its full $N^s - 2$ dimensionality rather than a point at a time. However, because eqs 28 and 29 are based on perturbation theory their validity is limited to a neighborhood of the conical intersection $\mathbf{R}^x$ used as the origin of the perturbation expansion. When $M\,\zeta_i$ are small eqs 28 and 29 yield a locus of confluences of dimension $M - 1$. For $M < N^s - 1$, the predicted dimension of the locus of confluences is less than $N^s - 2$. This can occur for several reasons. The most obvious reason is that along some directions we are far from a confluence. In this situation, eqs 28 and 29 can be used in an iterative manner as outlined in section 3. On the other hand, the inadequacy of perturbation theory might reflect a seam that does not achieve its full dimensionality or the failure of the linear seam approximation (see section 3).

3. Results and Discussion

In this section, the ideas and methods discussed above are used to study in detail the vicinity of $\mathbf{R}^c$ for BH_2 and HNCO.

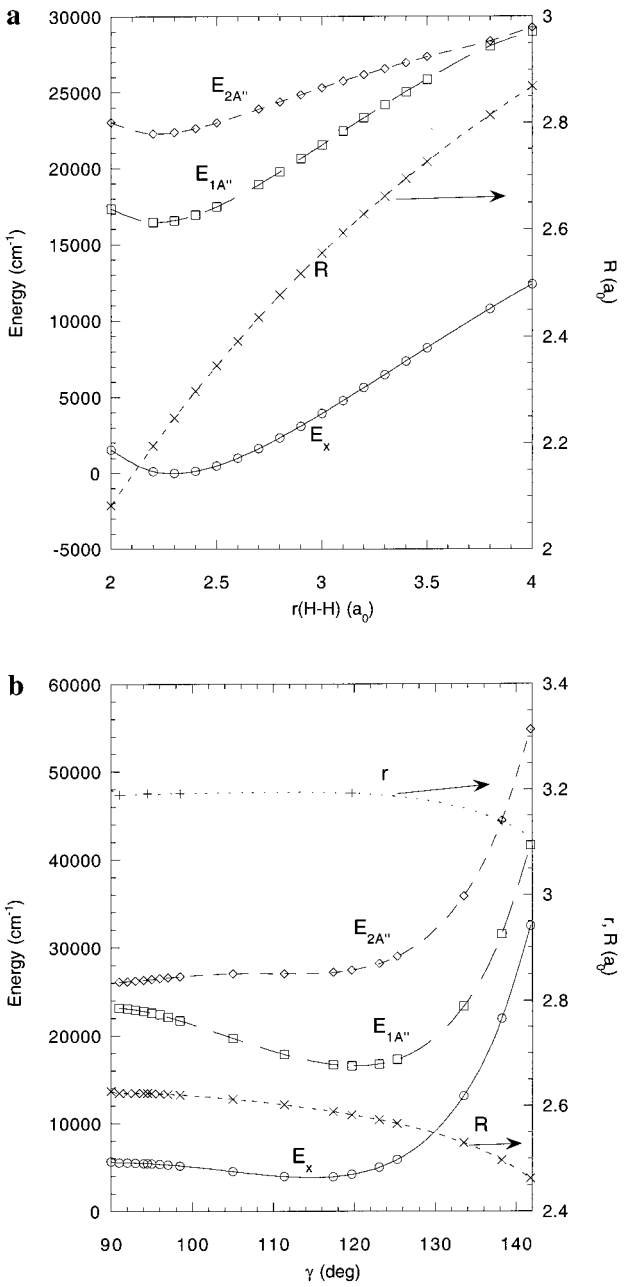

Figure 4. In BH_2 (a) R and the energies of the seam of conical intersection E_x and the two lower $^2A''$ states, $E_{1^2A''}$, $E_{2^2A''}$ along r, in C_{2v} symmetry (b) R, r, and the energies of the seam of conical intersection E_x and the two lower $^2A''$ states, $E_{1^2A''}$, $E_{2^2A''}$ along γ, in C_s symmetry.

The multireference configuration interaction descriptions for BH_2 and HNCO have been reported previously.[7,8] Geometries for BH_2 are given in terms of Jacobi coordinates $\mathbf{R} = (R, r, \gamma)$ where R is the distance between B and the center of mass of H_2 in a_0, r is the H_2 distance in a_0, and γ is the acute angle between the two line segments in degrees (see Figure 2). For HNCO, the reported geometries are given in internal coordinates $\mathbf{R} = (R(\text{N}-\text{H}), R(\text{C}-\text{N}), R(\text{C}-\text{O}), \angle\text{HNC}, \angle\text{NCO}, \angle\text{HNCO})$; all distances are in a_0 (see Figure 2).

3.1 Description of the $1,2^2A'$ and $1,2^2A''$ States of BH_2. The Seam of Conical Intersection. The three states of BH_2 that correlate with the asymptotic limit $B(^2P) + H_2$ are the $1^2A'$, $2^2A'$, and $1^2A''$ in C_s symmetry or $^2A_1$, $^2B_2$, and $^2B_1$ in C_{2v} symmetry. The ground state of BH_2 has $^2A_1$ symmetry with a minimum at $\mathbf{R}^g = (3.206, 4.059, 90°)$ and the van der Waals

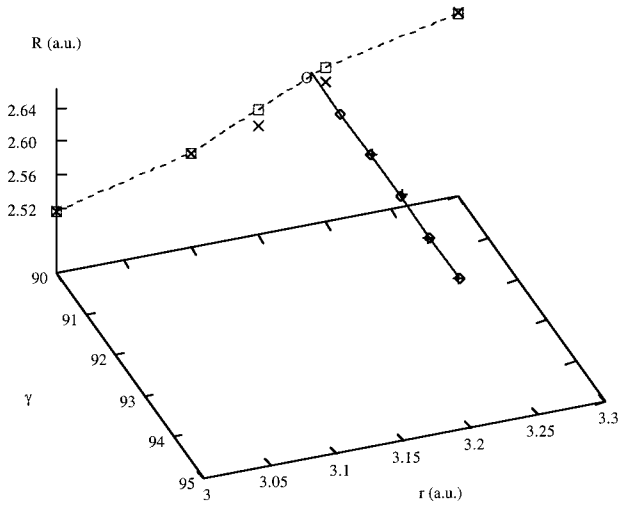

Figure 5. (r, R, γ) for the two branches of the seam near the confluence in BH_2. Points on the C_{2v} branch are squares and on the C_s branch are diamonds. × and + represent points predicted using the linear-seam approximation. O represents the predicted point of confluence from the nearby point (3.15, 2.61, 90) of the C_{2v} branch.

complex has symmetry $^2B_2$ with a minimum at $\mathbf{R}^{wdv} = (6.082, 1.405, 90°)$.[7] Thus, for C_{2v} symmetry a $^2A_1 - {}^2B_2$ seam of conical intersection is expected and indeed has been found, for the $1^2A'$ and $2^2A'$ states. Quite unexpected was a seam of conical intersection of these same two states for C_s symmetries which intersects the C_{2v} seam. Figure 4a and 4b reports for the C_{2v} and C_s branches of the seam respectively the geometry $\mathbf{R}^{x,C2v}$ and $\mathbf{R}^{x,Cs}$, together with energy $E_x(\mathbf{R}^x) \equiv E_{1^2A'}(\mathbf{R}^x) = E_{2^2A'}(\mathbf{R}^x)$. The energies $E_{1^2A''}(\mathbf{R}^x)$, $E_{2^2A''}(\mathbf{R}^x)$ are also plotted in these figures for a more complete picture of the energetics in this region. In C_{2v} symmetry for smaller r the $1^2A''$ state has $^2A_2$ symmetry, and the $2^2A''$ state has $^2B_1$ symmetry but the ordering switches after $r = 3.8a_0$. Here and below, the superscript identifying the seam branch will be suppressed when the branch is irrelevant or clear from the context. Figure 5 shows both branches and the confluence in a 3D plot (r, R, γ). The C_{2v} branch is in the (r, R) plane ($\gamma = 90$), whereas the C_s branch seam coordinate is dominated by γ.

3.2 Representing the Vicinity of the Seam. *3.2.1 General Features of a Confluence.* Figure 1 shows the potential energy surfaces for the crossing states in BH_2 in the vicinity of the conical intersections and the confluence, based on the analytic representations of the adiabatic energies given in eq 3 using parameters described below. This plot demonstrates the ability to represent continuously the surfaces along the seam and the confluence. For the first time, the unique shape of the surfaces due to the confluence is revealed. Figure 1a is a plot of the two surfaces along r (approximately, the seam coordinate z in the C_{2v} seam) and the intersection adapted coordinate y in the C_{2v} seam. These two coordinates switch roles for the C_s seam facilitating the depiction of the confluence. Figure 1b is a plot of the same two surfaces along r and the intersection adapted coordinate x. In this coordinates the confluence does not appear in contrast to the previous plot where it is obvious. In Figure 1b, the two surfaces are always separated for $x \neq 0$, whereas in Figure 1a, the surfaces flatten and at the confluence become degenerate even for $y \neq 0$. Another important observation that emerges from these figures and will be discussed further below is that the second-order effects become preeminent near the confluence. Thus, the cone in Figure 1a is curved, whereas in Figure 1b, the linear terms are dominant. A detailed discussion of the first and second-order parameters follows.

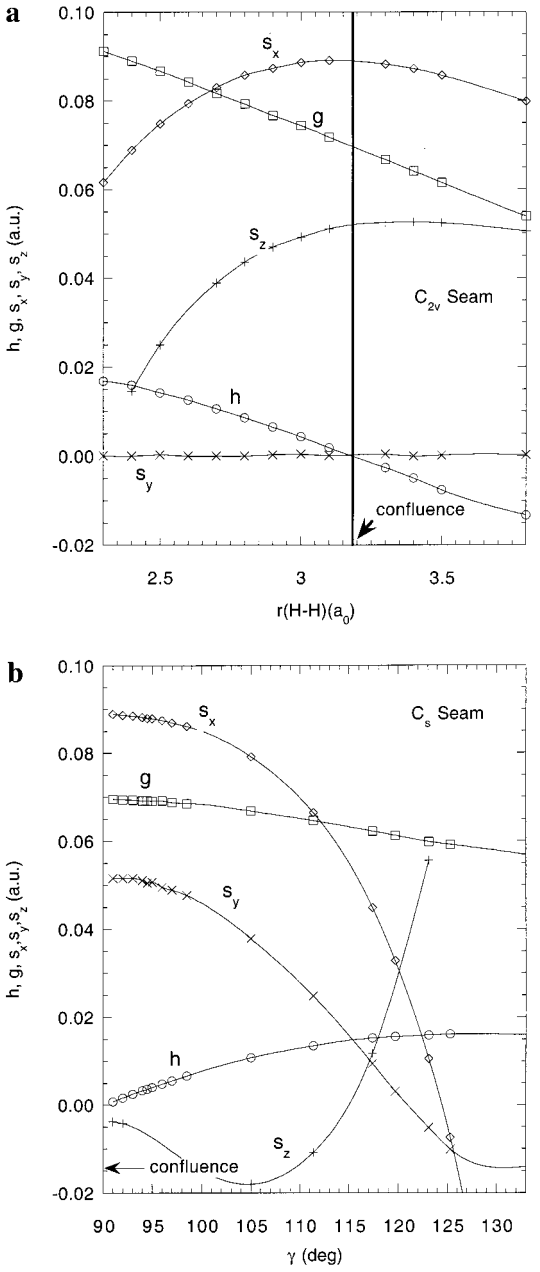

Figure 6. First-order parameters g, h, s_x, s_y, s_z of the seam in BH_2 along (a) r in C_{2v} symmetry (b) γ in C_s symmetry.

3.2.2 First-Order Parameters. The energy and derivative couplings near a point of conical intersection are well described by the first and second-order parameters. These parameters in general will not be continuous along the seam. This lack of continuity, which is attributable to the invariance of the degenerate electronic states with respect to a rotation, complicates their use for a global representation of the seam. As described elsewhere the use of orthogonal $\mathbf{g}^{IJ}$ and $\mathbf{h}^{IJ}$ circumvents this difficulty. These are derived from the "nascent" $\mathbf{g}^{IJ}$ and $\mathbf{h}^{IJ}$ by a rotation of the degenerate wave functions that orthogonalizes them.[26] This procedure should be distinguished from one which merely orthogonalizes $\mathbf{g}^{IJ}$ and $\mathbf{h}^{IJ}$. In that case, the energy in eqs 3 necessarily changes form. Figure 6a and 6b reports the first-order parameters g, h, and s_w,$(w = x, y, z)$ along the C_{2v} and C_s branches of the seam. For C_{2v}, symmetry $s_y = 0$. From eq 3, these parameters determine the conical shape of the energy surface moving away from the seam along the g−h plane. The topography of the cone is characterized by the

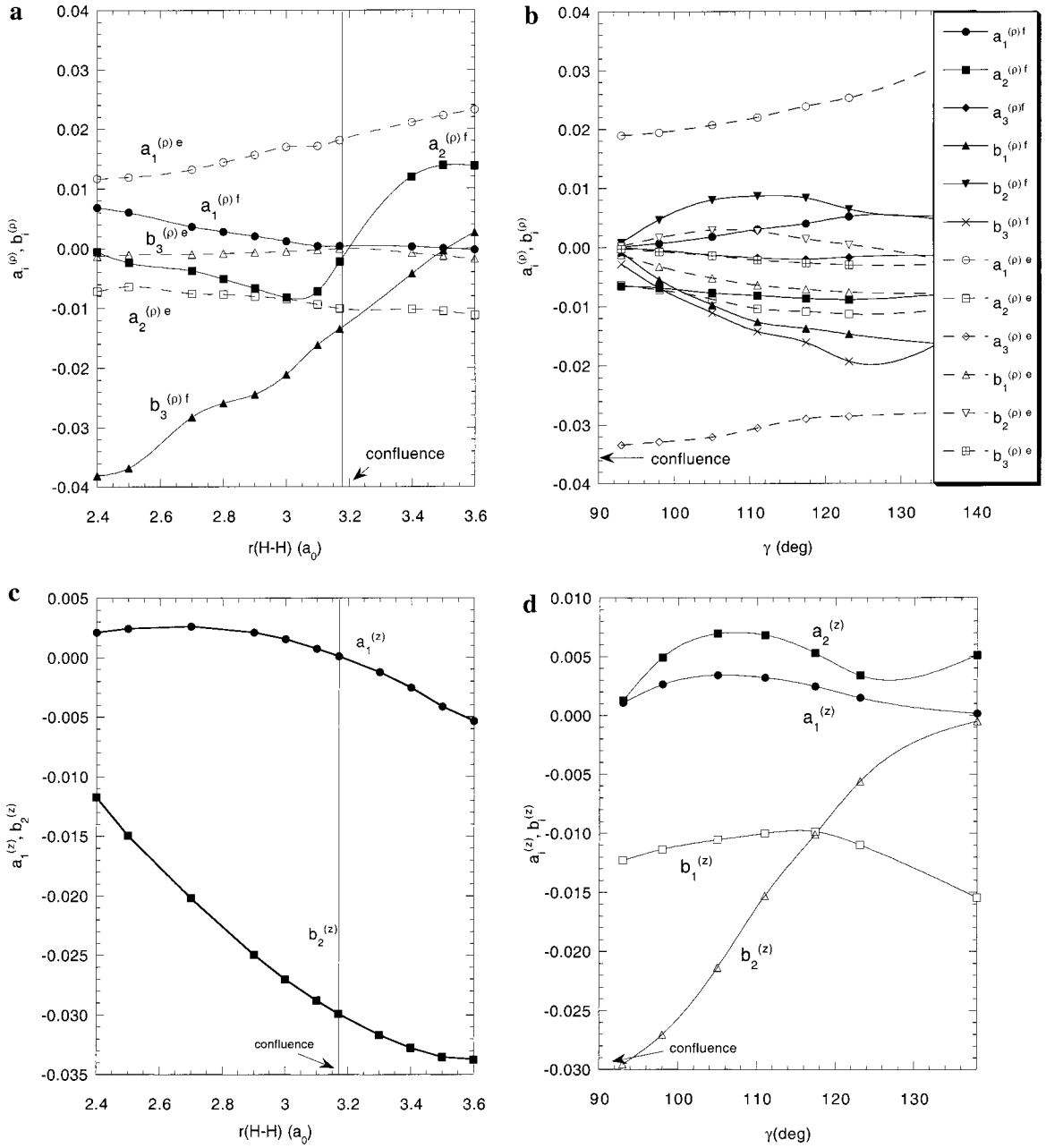

Figure 7. Second-order parameters $a_i^{(\rho)}$, $b_i^{(\rho)}$ obtained by fitting f_ρ (denoted by superscript f) and ΔE (denoted by superscript e) along (a) r in C_{2v} symmetry (b) γ in C_s symmetry. Second-order parameters $a_i^{(z)}$, $b_i^{(z)}$, obtained by fitting f_ρ along (c) r in C_{2v} symmetry (d) γ in C_s symmetry.

magnitude of these parameters.[27] In order for the energy to be continuous along the seam including the confluence, these parameters have to be continuous also. This is seen in Figure 6a and 6b. Approaching the confluence the parameters determining the individual branches approach each other. Notice that the y and z coordinates switch roles at the confluence as discussed in section 2. Then at the confluence $g(\tau^{x,C2v}) = g(\tau^{x,Cs})$, $s_x(\tau^{x,C2v}) = s_x(\tau^{x,Cs})$, $h(\tau^{x,C2v}) = h(\tau^{x,Cs}) = 0$, but $s_y(\tau^{x,C2v}) = s_z(\tau^{x,Cs})$ and $s_z(\tau^{x,C2v}) = s_y(\tau^{x,Cs})$.

3.2.3 Second-Order Parameters. It was seen in Section 2 that the second order terms are readily described in analytic form by subtracting out the first-order contributions in the expressions for the energy and the derivative coupling. Thus, the second-order parameters are obtained from eqs 23,24 as described in section 2.5.

The parameters $a_i^{(\rho)}$, $b_i^{(\rho)}$, obtained by fitting the energy differences or the derivative couplings along the C_{2v} and C_s branches respectively are shown in Figure 7a,b. The parameters $a_i^{(z)}$, $b_i^{(z)}$, obtained by fitting the derivative couplings are shown in Figure 7c,d. The $a_i^{(z)}$, $b_i^{(z)}$ parameters play an important role in the existence and location of confluences as described in section 2.6.1.

To examine the differences between the two fitting procedures two points along the C_{2v} branch were chosen and studied in detail. The energy differences and derivative couplings were plotted using (a) the ab initio values, denoted as $\Delta E^{(2,ab)}$, $\mathbf{f}^{(ab)}$; (b) the perturbation theory expressions using parameters obtained by fitting the derivative coupling f_ρ, denoted as $\Delta E^{(2,f)}$, $\mathbf{f}^{(f)}$; and (c) the perturbation theory expressions using parameters obtained by fitting the second-order energy difference $\Delta E^{(2)}$, denoted as $\Delta E^{(2,e)}$, $\mathbf{f}^{(e)}$. These three methods will be denoted *ab*, *f*, *e* respectively. Note that whenever the methods *f*, *e* will be specified, the superscripts 2, 2′ will be droped from **f**.

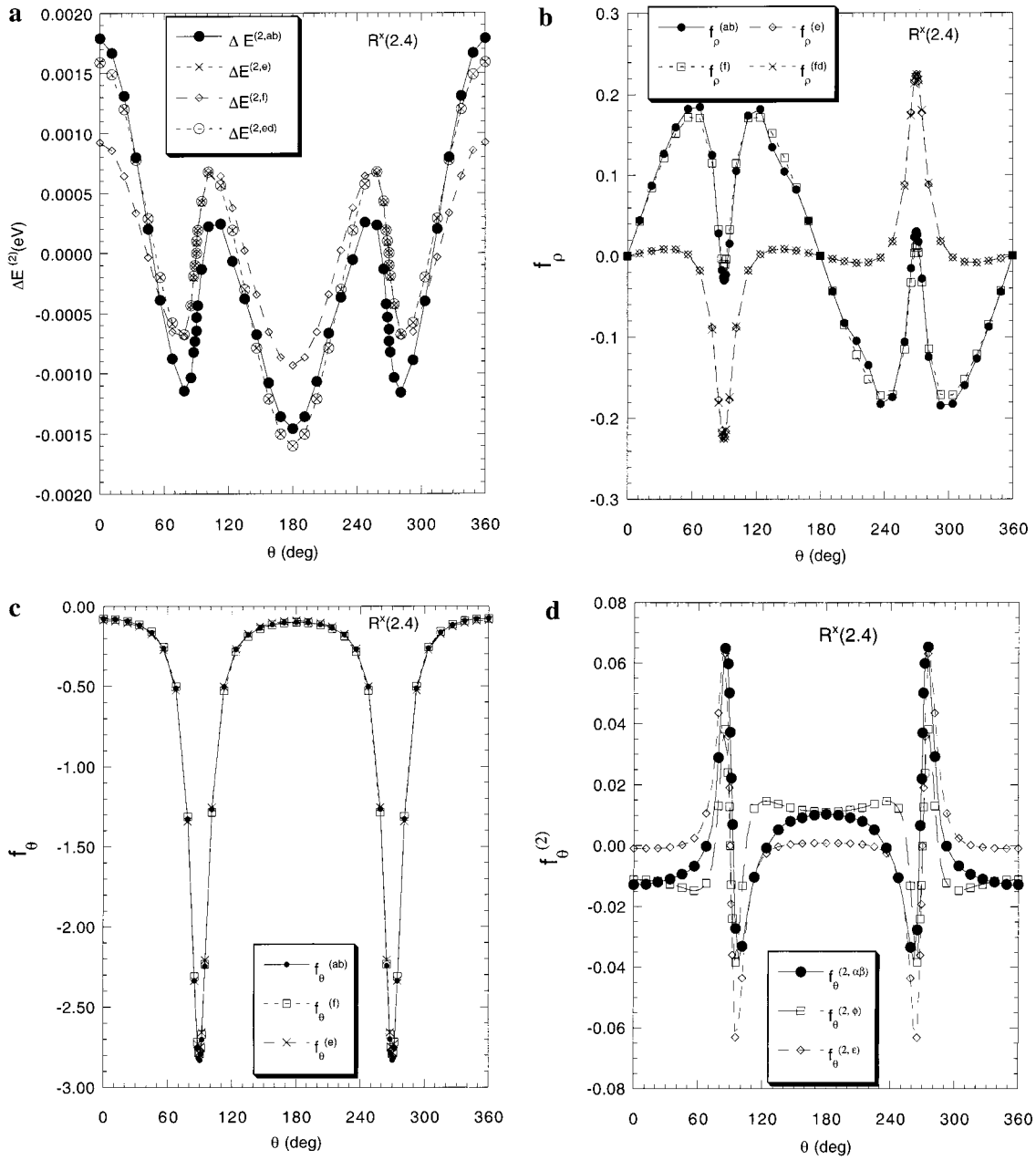

Figure 8. At $\mathbf{R}^x(2.4)$ for $\rho = 0.05$ and $0 < \theta < 2\pi$: (a) $\Delta E^{(2,m)}$), $m = ab, f, e, ed$, (b) $f_\rho^{(m)}$, $m = ab, f, e, fd$, (c) $f_\theta^{(m)}$, $m = ab, f, e$, (d) $f_\theta^{(2,m)}$, $m = ab, f, e$.

It should be mentioned that Figures 8 and 9 below can be misleading suggesting large discrepancies between the calculated and fitted energies and derivative coupling because the scale in these figures is small. Thus, even when differences appear large the absolute differences are small on the order of tens of wavenumbers.

The first point is close to the minimum energy point of the C_{2v} branch, at $\mathbf{R}^x(2.4) = (2.30, 2.4, 90)$. For this point, a large number of θ values were used to confirm convergence with respect to θ integrals. Figure 8a reports $\Delta E^{(2,m)}$, $m = ab, f, e$. In addition, the second-order energy difference $\Delta E^{(2,ed)}$ was calculated using the diabatic representation (by subtracting the first-order energy (eq 8 from eq 21), but with parameters obtained from fitting the adiabatic energy. $\Delta E^{(2,f)}$ and $\Delta E^{(2,e)}$ agree with $\Delta E^{(2,ab)}$, although $\Delta E^{(2,e)}$ gives better agreement as expected. The largest discrepancies for $\Delta E^{(2,f)}$ occur at $\theta = 0$, 180°. $\Delta E^{(2,e)}$ and $\Delta E^{(2,ed)}$ are virtually identical which is not unexpected because the two representations are identical to second order as shown in eq 22.

Figure 8b reports $f_\rho^{(m)}$, $m = ab, f, e$. Here, a diabatic expression $f_\rho^{(fd)}$ is given by the derivative of the angle of rotation Θ from adiabatic to diabatic representation,[22] $f_\rho^{(fd)} = \partial\Theta/\partial\rho$ where Θ is given by eq 15. The parameters are obtained by fitting f_ρ. The difference between $f_\rho^{(e)}$ and $f_\rho^{(ab)}$ is relatively large when compared with $f_\rho^{(f)}$ which agrees well with $f_\rho^{(ab)}$. The largest discrepancies occur at $\theta = 90°$, 270°. $f_\theta^{(m)}$, $m = ab, f, e$ are plotted in Figure 8c where good agreement is evinced. The reason for this is that the largest term in f_θ is the first-order contribution which is independent of $a_i^{(\rho)}$, $b_i^{(\rho)}$. A more precise comparison can be made if this term is subtracted from the derivative coupling and only the second order terms are left. This is shown in Figure 8d. Here, the differences appear again, although not so strikingly as in f_ρ. This should be expected

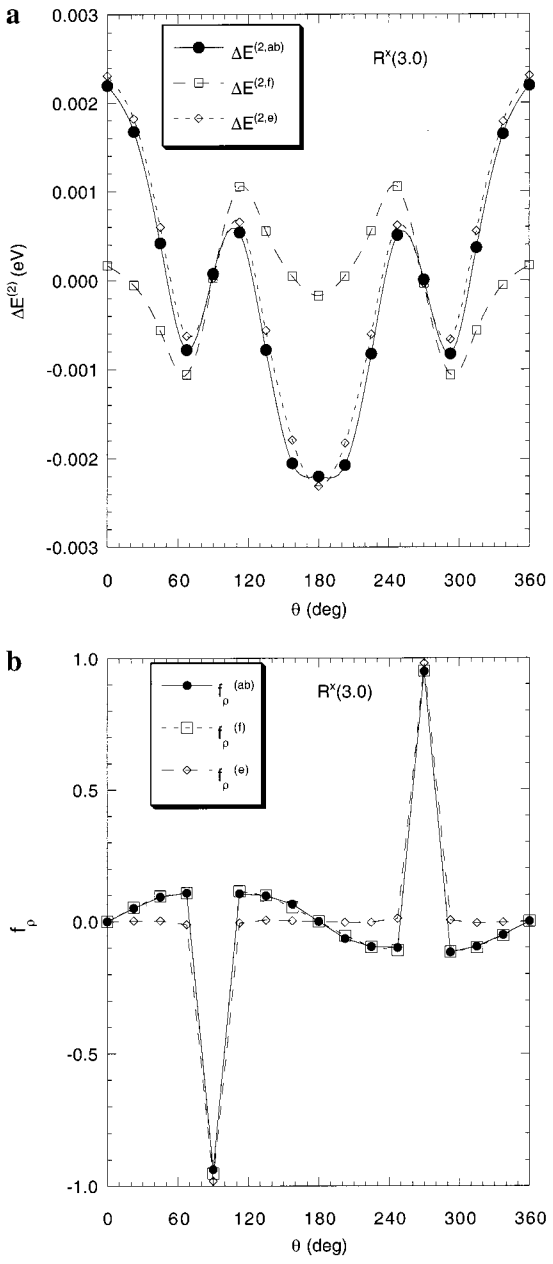

Figure 9. (a, b) Same as 9a, b at $\mathbf{R}^x(3.0)$

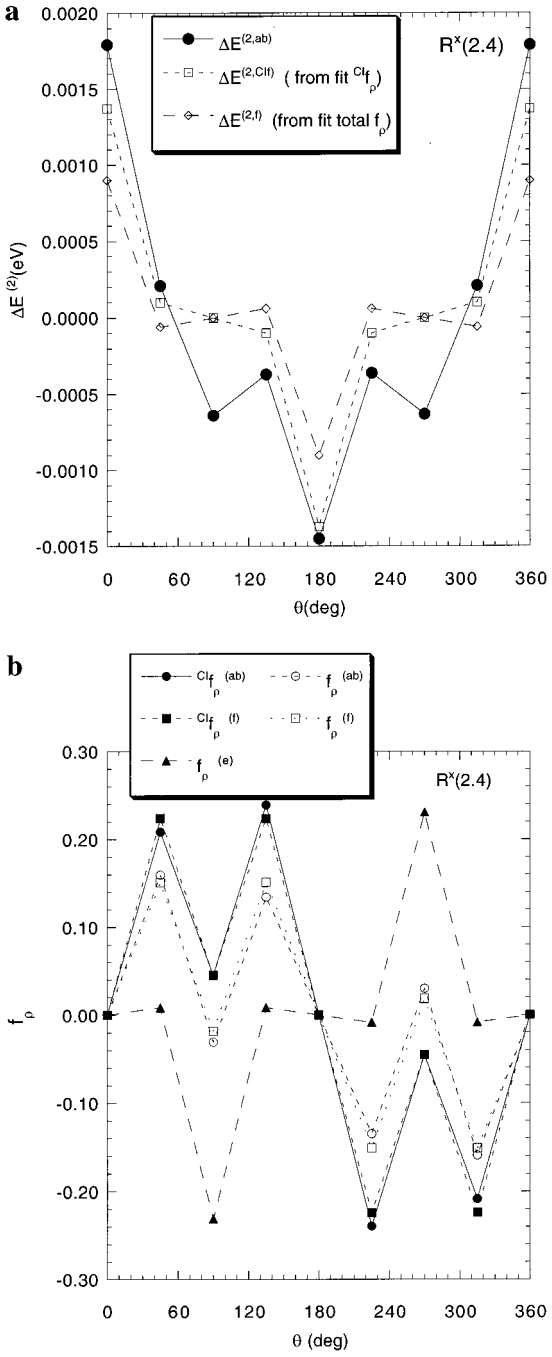

Figure 10. At $\mathbf{R}^x(2.4)$ for $\rho = 0.05$ and $0 < \theta < 2\pi$: (a) $\Delta E^{(2,m)}$, $m = ab$, ^{CI}f, f (b) $f_\rho^{(ab)}$, $f_\rho^{(f)}$, $^{CI}f_\rho^{(ab)}$, $^{CI}f_\rho^{(f)}$.

because $f_\rho^{(2)}$ and $f_\theta^{(2)}$ depend on the same parameters, as seen in eqs 11,13. In some parts, $f_\theta^{(2,f)}$ agrees better with $f_\theta^{(2,ab)}$ but in other parts $f_\theta^{(2,e)}$ works better.

The other point studied is chosen close to the confluence and is $\mathbf{R}^x$ (3.0) = (2.55,3.0,90). For this point only the energy and f_ρ plots will be shown since the f_θ plots do not include additional information. The corresponding plots for $\mathbf{R}^x$ (3.0) are shown in Figures 9a,b. The fits are quite different than before. $\Delta E^{(2,f)}$ differs from $\Delta E^{(2,ab)}$ substantially. The derivative couplings are described well independently of the origin of the parameters. The second-order contributions to the derivative coupling at this point, measured by f_ρ, are much larger than those at the previous point $\mathbf{R}^x$ (2.4). This is a consequence of being near the confluence and will be discussed further in Section 3.4. The larger magnitude of these terms, however, makes them easier to describe as the good agreement in Figure 9b shows.

Although the differences discussed above are small, it is useful to try to understand their origin. As was discussed in Section 2, the derivative coupling consists of two terms but the perturbation theory expressions describe only the CI part. If the CSF part is non negligible, the perturbation theory will be inadequate to describe the derivative coupling. This could cause the observed discrepancy between the parameters obtained from fitting the derivative coupling or the energy difference. At $\mathbf{R}^x(2.4)$ **a** and **b** were determined using $^{CI}f_\rho$. Figure 10a,b shows $\Delta E^{(2)}$ and f_ρ from the calculations and the fitting. In Figure 10a $\Delta E^{(2,CIf)}$ calculated using parameters from fitting $^{CI}f_\rho$ agrees much better with $\Delta E^{(2,ab)}$, than $\Delta E^{(2,f)}$. There is no improvement however in the agreement between $f_\rho^{(e)}$, and $^{CI}f_\rho^{(ab)}$. To the contrary, it becomes worse, indicating that higher order effects contribute to the energy that cannot be eliminated here.

It is interesting to note that in general the discrepancies are larger at the points $\theta = 0$, 90, 180, 270°. In this regard, note that the energy difference becomes zero at $\theta = 90°$, 270° and

TABLE 1: For a Point on the Seam (R^x, r^x, 90) *gh*, ΔE, the Slope of the Seam Expressed as $R'(r_i) = (R_{i+1} - R_i)/(r_{i+1} - r_i)$, and the Change in the Slope $d(R'(r_i))/dr = R'(r_{i+1}) - R'(r_i)/(r_{i+1} - r_i)$ are Given. Energies are Given in cm^{-1} and Distances in a_0

R^x	r^x	gh	ΔE	R'	$dR'(r)/dr$
2.4769	2.8	0.6837(−3)	0.01	0.402	0.16
2.5171	2.9	0.4951(−3)	0.04	0.386	0.16
2.5557	3.0	0.3205(−3)	0.22	0.370	0.12
2.5927	3.1	0.1333(−3)	0.44	0.358	0.12
2.6106	3.15	0.5264(−4)	0.006	0.352	0.34
2.6282	3.2	−0.2805(−4)	0.88	0.335	0.03
2.6618	3.3	−0.1740(−3)	6.58	0.332	0.17
2.6950	3.4	−0.3175(−3)	0.04	0.315	0.12
2.7265	3.5	−0.4666(−3)	0.006	0.303	
2.7568	3.6	0.5537(−3)	0.01		

has the value of $\Delta E^{(2)} = 2a_1^{(\rho)}$ at $\theta = 0°, 180°$. f_ρ vanishes at $\theta = 0°, 180°$ and is given by $f_\rho = -a_2^{(\rho)}/2q$ at $\theta = 90°, 270°$. These expressions show that $\Delta E^{(2)}$ and f_ρ depend on only one parameter at these extreme points, so they will be particularly sensitive to the fitting procedure. $a_1^{(\rho)}$ obtained from the two fits differ the most at $\mathbf{R}^x(3.0)$, and this will lead to the energy difference being worst described at $\mathbf{R}^x(3.0)$; $a_2^{(\rho)}$ and $b_3^{(\rho)}$ differ the most between the two fits at $\mathbf{R}^x(2.4)$ and this causes the derivative coupling to be worst described at $\mathbf{R}^x(2.4)$.

Although this discussion leads to the conclusion that higher order effects can lead to differences in energy-based and derivative-coupling-based results, the differences are not large and they decrease with increasing size of the second order terms. The largest part of the derivative coupling is the first order term which gives good agreement. Only when one separates the different contributions one is able to notice the differences. The analysis presented here based on the intersection adapted coordinates enables this separation and detection of any differences. Further, the analysis indicate that the best way to eliminate as much as possible the small differences in $\Delta E^{(2,e)}$ and $\Delta E^{(2,f)}$ is by fitting ${}^{CI}\mathbf{f}$ rather than $\mathbf{f}$. If very precise values for $\mathbf{f}$ are required ${}^{CSF}\mathbf{f}$ can be added subsequently.

3.3 Locating Confluences. In the pointwise approach the vanishing of h is used to identify a confluence. Using this approach, the point of confluence for BH_2 was located at $\mathbf{R}^c \equiv (R^c, r^c, \gamma^c) = (2.621, 3.182, 90°)$. This point is given more precisely than before.[7] Table 1 illustrates the pointwise search and considers the range of validity of the linear seam approximation. The magnitude *gh* along $\mathbf{R}^x$ is monitored to find $\mathbf{R}^c$. The slope of the seam line $R'(r_i) \equiv dR(r_i)/dr = (R_{i+1} - R_i)/(r_{i+1} - r_i)$ is given in Table 1. Seam curvature is indicated by a non constant slope, as measured by the change of the slope $dR'(r_i)/dr_i = R'(r_{i+1}) - R'(r_i)/(r_{i+1} - r_i)$ also given in Table 1. It is expected and indeed found that seam curvature limits the accuracy of $\mathbf{R}^{c,p}$. Figure 5 compares the actual seam with the seam predicted using the linear approximation and extrapolating from a previous point. The predicted points are in good agreement with the actual points.

The iterative method for locating confluences using eqs 28, 29 is illustrated in Table 2. In the following discussion a subscript 1 or 2 will be used in $\mathbf{R}$ to denote a BH_2 geometry or an HNCO geometry, respectively. Starting from a point $\mathbf{R}_1^{x1}$=(2.434, 2.7, 90) eq 29 was used to predict a point closer to the confluence. This point, $\mathbf{R}_1^{x2}$, gives a *gh* still too large to represent a confluence but it can be used as an improved approximate origin to construct $\mathbf{H}^{(d)}$. Because ΔE for $\mathbf{R}_1^{x2}$ is large we have to move closer to the seam before we use this point as the origin. This is $\mathbf{R}_1^{x2r}$ obtained from a single iteration of the conical intersection search algorithm, giving $\Delta E = 4.1$ cm^{-1}. Here, the superscript r will be added to indicate that a point has been relaxed to come closer to the seam. Starting from $\mathbf{R}_1^{x2r}$ eq 29 is used to predict $\mathbf{R}_1^{x3}$ which gives *gh* an order of magnitude smaller. One more iteration gives a point $\mathbf{R}_1^{x4}$ that can be considered as the confluence. Comparing Tables 1 and 2 illustrates the potential utility of the iterative method.

TABLE 2: Points R_1^x on the $1^2A' - 2^2A'$ Seam of Conical Intersection of BH_2 Using the Iterative Method to Locate the Confluence. Energies are Given in cm^{-1} and Distances in a_0

R	r	gh	ΔE	z
$\mathbf{R}_1^{x1}$: 2.434	2.70	0.8655(−3)	0.012	0.524
$\mathbf{R}_1^{x2}$: 2.721	3.364	0.2647(−3)	810	
$\mathbf{R}_1^{x2r}$: 2.695	3.399	0.3169(−3)	4.1	0.151
$\mathbf{R}_1^{x3}$: 2.630	3.199	0.2732(−4)	62.17	
$\mathbf{R}_1^{x3r}$: 2.629	3.202	0.3184(−4)	0.014	0.0154
$\mathbf{R}_1^{x4}$: 2.622	3.1815	0.6015(−5)	0.56	

HNCO being a larger system benefits more from this method. Confluences for cis nuclear configurations of HNCO were considered starting from $\mathbf{R}_2{}^{x1}$ = (1.936, 2.67, 2.27, 117.3, 111.40, 180), which based on the results of Ref. 26 is expected to be near a confluence. The results from an analysis using second-order parameters, obtained using a loop centered at $\mathbf{R}_2^{x1}$ with $\rho = 0.05\ a_0$, and solving eq 29 are reported in Table 3. The dimension of the seam here is 4 and the dimension of the locus of confluence may be as large as 3 complicating its determination substantially. First, observe that ζ_i, $i = 1 - 3$ are quite large contraindicating their utility and that $\boldsymbol{\tau} = (0, 0, 0, 0, \zeta_4)$ is farther than expected from $\mathbf{R}_2^{x1}$. As currently implemented, the ζ_i are determined from $\mathbf{z}^i$ which are determined without regard to their role in these equations. It is often necessary to use linear combinations of the $\mathbf{z}^i$ to obtain ζ_i which are small. Seeking the direction of the seam that minimizes the distance from a predicted point of confluence, we construct the linear combination $\mathbf{z}^A = (0.26\zeta_1, 0.17\zeta_2, 0.0\zeta_3, 0.57\zeta_4)$ which yields, a $\boldsymbol{\tau}_2^{x2} = (0, 0, \mathbf{z}^A)$ near $\mathbf{R}_2^{x1}$. Although $gh(\tau_2^{x2}) = 0.443(10^{-3})$ is too large to represent confluence, $\boldsymbol{\tau}_2^{x2}$ can be used as an improved approximate origin for constructing $\mathbf{H}^{(d)}$. As in BH_2 ΔE is large so a point of conical intersection, $\boldsymbol{\tau}_2^{x2r}$ with $\Delta E < 1\ cm^{-1}$ was located near $\boldsymbol{\tau}_2^{x2}$ and used as the origin for constructing $\mathbf{H}^{(d)}$. In the resulting displacements, two comparatively small ζ_i exist indicating a confluence subspace of at least dimension 1 (see eq 28). One point of confluence was located by taking $\boldsymbol{\tau}_2^{x3} = (0, 0, \mathbf{z}^B)$ where $\mathbf{z}^B = (0\zeta_1, 0\zeta_2, 0.5\zeta_3, 0.5\zeta_4)$ based on $\mathbf{H}^{(d)}(\boldsymbol{\tau}_2^{x3})$. This point provides an order of magnitude improvement in *gh* over the results based on $\boldsymbol{\tau}_2^{x2}$ and is taken as a $\boldsymbol{\tau}^c$. More points of confluence can be found using different linear combinations of ζ_i.

3.4 Effect of the Confluence. It was demonstrated in Section 2.6.2 that one of the more interesting aspects of a confluence is the suppression of the geometric phase effect. Figure 3 illustrates this suppression near the cis confluence in HNCO reporting $f_\theta \approx (d/d\theta)\Theta(\mathbf{R})$ along a circle of radius ρ centered at $\mathbf{R}^{xs} = (R(H - N), 2.67, 2.271, 107, 106, 0.015)$. $\chi(f_\theta)$ is approximately 0. As a consequence $\Theta(2\pi) = \Theta(0)$ and there is no geometric phase effect. Note that the small circulation results from the sign change in f_θ near $\theta = \pi$. Approaching the confluence, the magnitude of h approaches zero and this affects the behavior of the derivative coupling. From eqs 6,13 the first-order derivative coupling along θ is given by the expression

$$f_\theta^{(1)}(\theta) = \frac{gh}{2q^2(\theta)} \tag{35}$$

TABLE 3: Points $\mathbf{R}_2^x$ on the $1^1A - 2^1A$ Seam of Conical Intersection of HNCO Using the Iterative Method to Locate the Confluence. Energies are Given in cm^{-1} and Distances in a_0. $z^A = (0.26\zeta_1, 0.17\zeta_2, 0.0, 0.57\zeta_4)$, $z^B = (0, 0, 1/2\zeta_3, 1/2\zeta_4)$

R(H−N)	R(C−N)	R(C−O)	∠HNC	∠NCO	gh	ΔE	ζ_i|i
$\mathbf{R}_2^{x1}$: 1.936	2.67	2.27	117.3	111.40	0.927(−3)	0.082	
2.063	2.929	2.418	49.7	102.2			1.901|1
3.666	2.840	2.240	93.2	108.4			1.369|2
1.822	3.744	0.618	94.8	97.2			1.306|3
1.912	2.492	2.176	130.8	99.8			0.379|4
$\mathbf{R}_2^{x2}$: 1.968	2.644	2.272	104.0	102.2	0.443(−3)	280	z^A
$\mathbf{R}_2^{x2r}$: 1.966	2.6617	2.287	103.3	102.4	0.362(−3)	0.062	z^{Ar}
2.636	2.597	2.227	35.1	104.1			2.234|1
0.279	2.688	2.327	139.1	103.5			−1.540|2
2.003	2.708	2.193	99.0	107.1	0.141(−4)	458	0.119|3
2.010	2.540	2.404	103.6	105.8	0.556(−4)	577	0.135|4
$\mathbf{R}_2^{x3}$: 2.007	2.623	2.298	101.2	106.5	0.409(−4)	309	z^B
$\mathbf{R}_2^{x3r}$: 1.997	2.648	2.313	100.7	106.2	0.375(−4)	4.20	z^{Br}

The extrema will occur when $(\partial f_\theta^{(1)}/\partial\theta = 0)$ $\sin\theta = 0$ or $\cos\theta = 0$. At $\sin\theta = 0$ there is a minimum given by $f_{\theta(\min)}^{(1)}(0) = h/2g$ and at $\cos\theta = 0$ there is a maximum given by $f_{\theta(\max)}^{(1)}(\pi/2) = g/2h$. As h approaches zero $f_{\theta(\min)}^{(1)}(0)$ approaches zero, whereas $f_{\theta(\max)}^{(1)}(\pi/2)$ approaches infinity. Thus, close to the confluence the largest derivative coupling occurs along the $\mathbf{h}^{IJ}$ direction and the smallest along the $\mathbf{g}^{IJ}$ direction (away from the confluence the difference between the two directions is not so sharp). Figure 11a,b shows the behavior of $f_{\theta(\min)}^{(1)}$ and $f_{\theta(\max)}^{(1)}$ approaching the confluence. Because of the small magnitude of h, the cone is very flat also in the same direction. These changes in the topography and the derivative coupling can affect the dynamics near the confluence. Transitions from one state to the other will be more probable along $\mathbf{h}^{IJ}$ but less probable in the whole space because $f_\theta^{(1)}(\theta)$ is small everywhere else and the probability of being near the $\mathbf{h}^{IJ}$ axis is small. To quantitatively study these effects wave packet calculations are needed.

The small magnitude of h near the confluence means that first-order terms depending on this quantity will be small giving the opportunity to second-order terms to dominate. This was seen in the curvature of the PES in Figure 1. For the derivative coupling, the increased importance of the second-order contributions are reflected in the larger values of f_ρ. This is confirmed in Figure 11a,b where the maximum absolute values of f_ρ along the seam coordinate are shown. The minimum value of q along θ, $q_{(\min)}$ is also shown in these figures. $q_{(\min)}$ occurs when $\sin\theta = 1$ and is equal to $|h|$, so it has a minimum at the confluence. Because $q_{(\min)}$ has a minimum at the confluence and is inversely proportional to f_ρ it drives this quantity into extrema. This behavior was observed also when individual points along the C_{2v} were discussed. We noticed there that the second-order terms at $\mathbf{R}^x(3.0)$ are larger than those at $\mathbf{R}^x(2.4)$. This observation is in agreement with our initial expectation that second-order terms become important as one approaches the confluence.

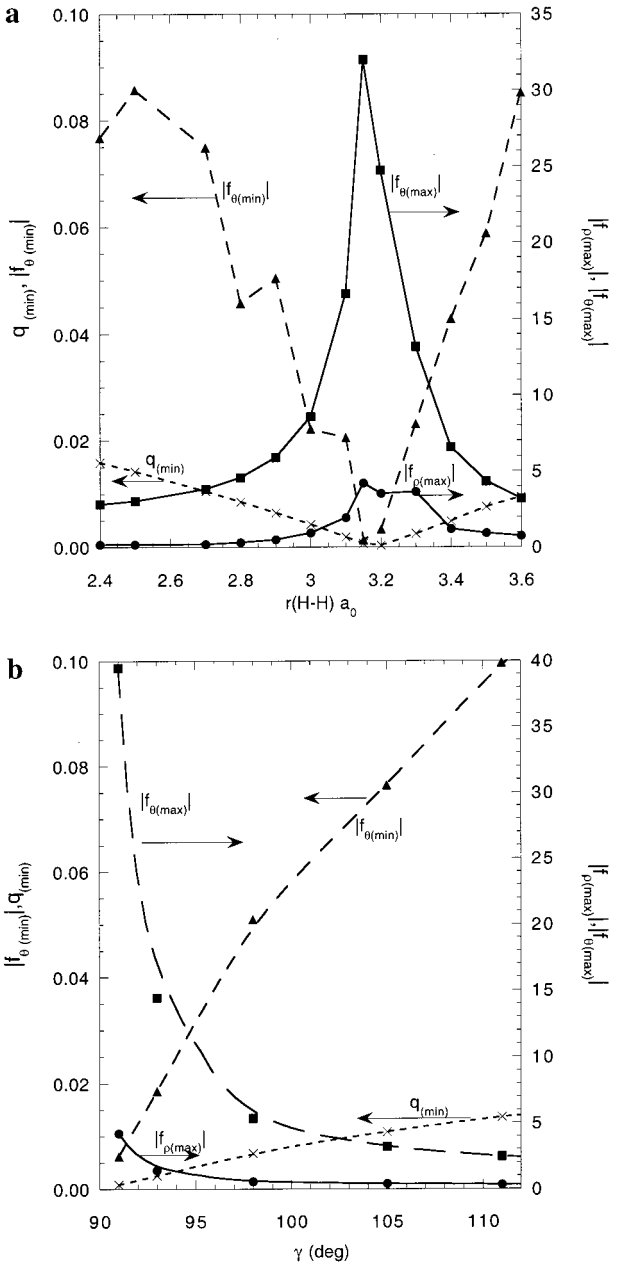

Figure 11. Absolute value of the maximum of f_θ and f_ρ along the loop. Absolute value of the minimum of f_θ, and $q_{(\min)}$ along the seam coordinate (a) in C_{2v} symmetry (b) in C_s symmetry.

4. Conclusions

Analytical expressions derived from perturbation theory have been used to represent energies and derivative couplings in the vicinity of a seam of conical intersection. We have investigated the validity of using potential energy-based descriptions to evaluate derivative couplings or using derivative-coupling-based approaches to evaluate energies. When the singular derivative coupling terms are subtracted out the remaining second-order terms are given by analytic expressions. Although the errors appear to be large because they are a significant percentage of the quantities, the absolute errors are small. This is so because the quantities described are the second-order terms which are in this case small. The agreement between the two methods

depends on the magnitude of these terms. As the second-order terms become larger the agreement improves. This enables a good description of the vicinity of the confluence where second-order terms are important.

The CSF part of the derivative coupling is negligible compared to the singular term which is isolated in a single component of the derivative coupling when the intersection adapted coordinates are used. However, the CSF part may contribute to the remaining components of the derivative coupling and this contribution has been investigated in this work.

The preeminence of second-order terms is one of the signature properties of a confluence. Derivative couplings show special behavior in the vicinity of the confluence, which may affect the dynamics of the interstate transitions. The sharp difference in $f_\theta^{(1)}$ between the directions $\mathbf{g}^{IJ}$ and $\mathbf{h}^{IJ}$ is an illustration of this special behavior. To be able to answer this question with more certainty, nuclear dynamics calculations should be performed. We are planning on studying the dynamics in the vicinity of confluences in the future.

An iterative method for locating confluences of conical intersection seams in systems with many atoms, using information at a point in the seam and the above analytical representations has been derived. This method has been tested using the known confluences on BH_2 and on the higher dimension system HNCO. It has been demonstrated to be a valuable tool for locating confluences.

Acknowledgment. This work was supported by AFOSR Grant No. F49620-99-1019.

References and Notes

(1) Yarkony, D. R. *J. Phys. Chem. A* **2001**, *105*, 2642−2645.
(2) Varandas, A.; Brown, F. B.; Mead, C. A.; Truhlar, D. G. *J. Chem. Phys.* **1987,** *86*, 6258−6269.
(3) Thompson, T. C.; Mead, C. A. *J. Chem. Phys.* **1985**, *82*, 2408.
(4) Thompson, T. C.; Iznirlian, G., Jr.; Lemon, S. J.; Truhlar, D. G.; Mead, C. A. *J. Chem. Phys.* **1985**, *82*, 5597−5603.
(5) Jordan, K. D. *Chem. Phys.* **1975**, *9*, 199.
(6) Abrol, R.; Shaw, A.; Kuppermann, A.; Yarkony, D. R. *J. Chem. Phys.* **2001**, *115*, 4640−4660.
(7) Glezakou, V.-A.; Gordon, M. S.; Yarkony, D. R. *J. Chem. Phys* **1998**, *108*, 5657−5659.
(8) Yarkony, D. R. *Mol. Phys.* **2001**, *99*, 1463−1467.
(9) Weeks, D. E.; Matsika, S.; Yarkony, D., work in progress.
(10) Alexander, M. *J. Chem. Phys.* **1993**, *99*, 6014−6026.
(11) Alexander, M.; Yang, M. *J. Chem. Phys.* **1995**, *103*, 7956−7965.
(12) Niday, T. A.; Weeks, D. E. *Chem. Phys. Lett.* **1999**, *308*, 106−114.
(13) Tam, S.; Macler, M.; DeRose, M. E.; Fajardo, M. E. *J. Chem. Phys.* **2000**, *113*, 9067−9078.
(14) Krumine, J. R.; Jang, S.; Alexander, M. H.; Voth, G. A. *J. Chem. Phys.* **2000**, *113*, 9079−9089.
(15) Mead, C. A. *J. Chem. Phys.* **1983**, *78*, 807−814.
(16) Thompson, T. C.; Mead, C. A. *J. Chem. Phys.* **1985**, *82*, 2408−2417.
(17) Yarkony, D. R. *J. Phys. Chem. A* **1997**, *101*, 4263−4270.
(18) Atchity, G. J.; Xantheas, S. S.; Ruedenberg, K. *J. Chem. Phys.* **1991**, *95*, 1862−1876.
(19) Yarkony, D. R. *Acc. Chem. Res.* **1998**, *31*, 511−518.
(20) Köppel, H.; Domcke, W.; Cederbaum, L. S. *Adv. Chem. Phys.* **1984**, *57*, 59−246.
(21) Yarkony, D. R. Molecular Structure. In *Atomic, Molecular and Optical Physics Handbook*; Drake, G. L., Ed.; AIP: New York, 1996.
(22) Yarkony, D. R. *J. Chem. Phys.* **2000**, *112*, 2111−2120.
(23) Lengsfield, B. H.; Yarkony., D. R. **1992**, *82*, 1−71.
(24) Yarkony, D. R. *J. Phys. Chem. A* **1998**, *102*, 8073−8077.
(25) Baer, M. *Mol. Phys.* **1980**, *40*, 1011−1013.
(26) Yarkony, D. R. *J. Phys. Chem. A* **2001**, *105*, 6277−6293.
(27) Yarkony, D. R. *J. Chem. Phys.* **2001**, *114*, 2601−2613.